Intriguing Low-Temperature Phase in the Antiferromagnetic Kagome Metal FeGe

M. Wenzel,[1,*] E. Uykur,[2] A. A. Tsirlin,[3] S. Pal,[1] R. Mathew Roy,[1] C. Yi,[4] C. Shekhar,[4] C. Felser,[4] A. V. Pronin,[1] and M. Dressel[1]

[1]*1. Physikalisches Institut, Universität Stuttgart, 70569 Stuttgart, Germany*

[2]*Helmholtz-Zentrum Dresden-Rossendorf, Institute of Ion Beam Physics and Materials Research, 01328 Dresden, Germany*

[3]*Felix Bloch Institute for Solid-State Physics, Leipzig University, 04103 Leipzig, Germany*

[4]*Max Planck Institute for Chemical Physics of Solids, 01187 Dresden, Germany*

(Received 23 January 2024; accepted 24 May 2024; published 28 June 2024)

The properties of kagome metals are governed by the interdependence of band topology and electronic correlations resulting in remarkably rich phase diagrams. Here, we study the temperature evolution of the bulk electronic structure of the antiferromagnetic kagome metal FeGe using infrared spectroscopy. We uncover drastic changes in the low-energy interband absorption at the 100 K structural phase transition that has been linked to a charge-density-wave (CDW) instability. We explain this effect by the minuscule Fe displacement in the kagome plane, which results in parallel bands in the vicinity of the Fermi level. In contrast to conventional CDW materials, however, the spectral weight shifts to low energies, ruling out the opening of a CDW gap in FeGe.

DOI: 10.1103/PhysRevLett.132.266505

The kagome lattice has been a fruitful playground to study novel quantum phenomena for over 70 years, uniting electronic correlations, topologically nontrivial states, and geometric frustration [1,2]. Being rooted in the network of corner-sharing triangles, destructive quantum interference results in localized states, i.e., a flat band over the entire Brillouin zone [3,4]. Together with the van Hove singularities at the M point, this can lead to exotic electronic orders, including flat-band ferromagnetism, Pomeranchuk instabilities, charge and spin bond order, unconventional superconductivity, nematicity, and Wigner crystallization [5–14].

Several of these intriguing phases have been identified in kagome metals, most prominently the exotic charge-density wave (CDW) in the superconducting AV_3Sb_5 (A = K, Rb, Cs) family [7,12,15–18]. Recently, charge order in the context of a magnetic kagome metal has been suggested as well [19–21]. Hexagonal FeGe crystallizes in the $P6/mmm$ space group featuring magnetic Fe-kagome planes stabilized by Ge1 atoms. Within one unit cell, these kagome layers are separated by a nonmagnetic honeycomb lattice of Ge2 atoms as visualized in Fig. 1(a). At room temperature, an out-of-plane antiferromagnetic (AFM) arrangement of the Fe-kagome layers is found, with ferromagnetically ordered Fe moments within the kagome planes. This AFM order persists down to approximately 60 K, below which a canted AFM arrangement with an additional reorientation at ∼30 K is observed [22,23].

More recent studies reveal an anomaly at $T_C \simeq 100$ K, where a slight drop in the in-plane magnetic susceptibility occurs [19,24,25]. However, no clear counterpart to this drop is observed in the electric resistivity [24,25]. Based on neutron diffraction and scanning tunneling microscopy (STM) measurements, a short-range-ordered CDW phase with a minor in-plane lattice distortion on the order of 10^{-4} of the kagome structure has been proposed [19,21,24]. Raman spectroscopy and neutron Larmor diffraction further suggested that deviations from the hexagonal symmetry occur already above T_C [26].

Although the low-temperature, putative CDW phase of FeGe was investigated extensively by surface-sensitive techniques such as STM and angle-resolved photoemission spectroscopy (ARPES), a systematic study of the temperature-dependent bulk electronic structure remains lacking. Fourier-transform infrared spectroscopy is one of the most effective approaches for investigating bulk CDW order [27–33]. Here, the gap opening at the Fermi level below T_{CDW} is normally manifested in a spectral weight transfer from low to high energies. However, our results on FeGe reveal no indication of a gap opening below T_C and, thus, contradict the CDW scenario at low temperatures. Aided by density functional theory (DFT) calculations of the band structure and the optical conductivity, we show that the reconstruction of the bands due to the structural transition at T_C leads to new interband optical transitions at low energies. We, thus, interpret the change in the electronic structure below T_C as band splitting rather than gap opening.

High-quality single crystals were synthesized as explained in Supplemental Material [34]. Prior to the optical experiments, we measured the in-plane magnetic susceptibility and dc resistivity of our samples. The results are plotted in Fig. S1(a) [34], confirming the stoichiometry and identifying the low-temperature anomaly at $T_C = 102$ K. Figure 1(b) displays the temperature-dependent real part of the in-plane

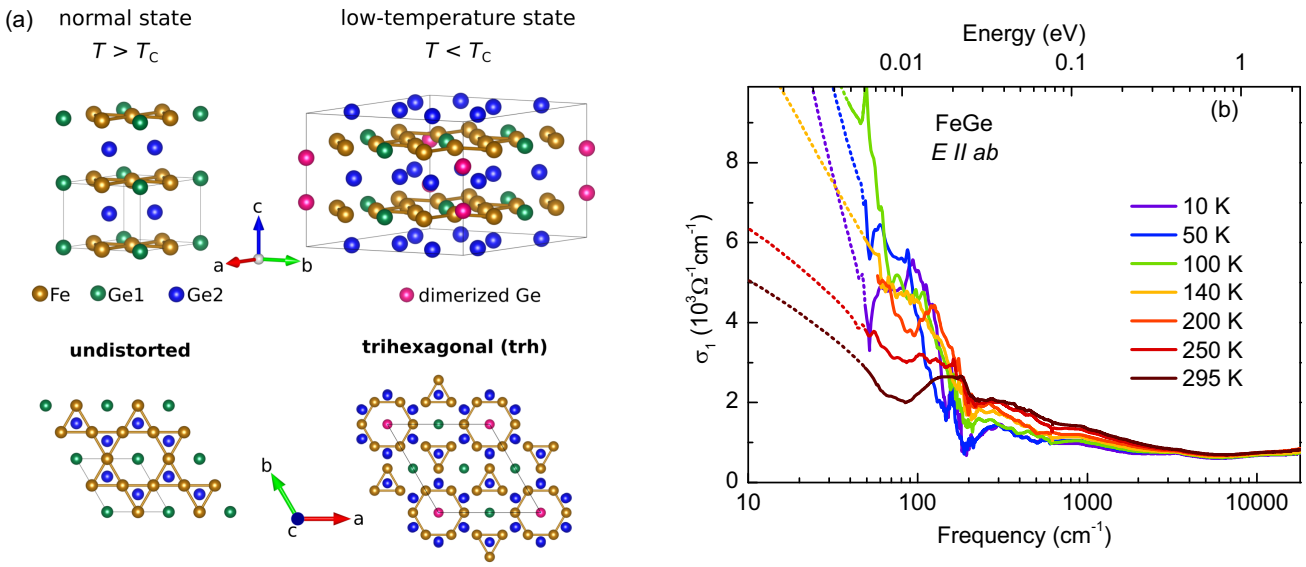

FIG. 1. (a) Crystal structure of hexagonal FeGe in the normal- and the low-temperature state. The bottom panel shows the undistorted in-plane Fe-kagome layer, as well as the trihexagonal distortion discussed in the literature [19]. The VESTA program was used for the crystal structure visualization [50]. (b) In-plane optical conductivity calculated from the measured reflectivity at selected temperatures with the dotted lines indicating the Hagen-Rubens extrapolations to low energies. See Fig. S1(d) [34] for the spectra at other temperatures.

optical conductivity. At first glance, the spectra resemble the optical spectra of other magnetic kagome metals such as the ferromagnetic Fe_3Sn_2 [47,48] and the ferrimagnetic RMn_6Sn_6 compounds [49]. However, it is apparent that the low-energy absorptions in FeGe strongly vary with temperature, including a new absorption feature around 100 cm^{-1} below T_C.

Using the Drude-Lorentz approach, different contributions to the total optical spectra are modeled, as shown in Fig. S2 [34] for selected temperatures. In addition to the classical Lorentzian (interband) and Drude (intraband) contributions, a sharp phonon mode around 190 cm^{-1} with a Fano-like shape and a temperature-dependent absorption peak at low energies are observed. The latter feature is assigned to the intraband signature of localized electrons (localization peak), in line with previous optical studies of kagome metals [47,49,51–54]. The total complex optical conductivity [$\tilde{\sigma} = \sigma_1 + i\sigma_2$] then takes the form

$$\tilde{\sigma}(\omega) = \tilde{\sigma}_{\text{intraband}} + \tilde{\sigma}_{\text{phonon}} + \tilde{\sigma}_{\text{interband}}. \quad (1)$$

To further visualize the temperature-driven changes in the low-energy interband absorptions, we subtract the Fano resonance and the intraband contributions, i.e., Drude and localization peaks, from the optical conductivities as presented in Figs. 2(a) and 2(b) for $T > T_C$. The room temperature data is reproduced by our DFT calculations given in Figs. 2(c) and 2(d) via raising the chemical potential by 110 meV. Upon cooling, the characteristic changes in the experimental spectra can be described by a systematic reduction of the chemical potential. This finding is consistent with the ARPES study in Ref. [19] reporting a significant shift of the chemical potential at temperatures above T_C. Aided by band-resolved optical conductivity calculations given in Supplemental Material [34], the variation of the low-energy spectral weight can be related to changes of the transition energy between multiple linear Fe $3d$ bands along $K \to \Gamma$, $\Gamma \to A$, and $A \to L$ [see Fig. 2(e)]. Note that, for all calculations, the energy axis needs to be rescaled by $1/2.1$ to achieve a good match with the experiment. A comparable rescaling factor of $1/1.6$ was observed in ARPES measurements [20]. Moreover, a similar discrepancy between theory and experiment is reported for other magnetic kagome metals, such as the RMn_6Sn_6 family and $Co_3Sn_2S_2$, signaling a significant influence of electronic correlations [49,55]. This effect is also observable in the difference between the experimental and DFT plasma frequencies, which can be used to gauge the strength of the electronic correlations as done in Fig. S8 [34]. Our data evidence much stronger correlations in FeGe compared to the nonmagnetic kagome metals, AV_3Sb_5 and ScV_6Sn_6, and even compared to the magnetic $Co_3Sn_2S_2$.

Upon cooling below T_C, several modifications in the electronic structure are clearly detected. First, the Fano resonance shifts to lower energies and significantly broadens upon approaching T_C, indicating strong electron-phonon coupling. This behavior is highly unusual for the temperature evolution of phonon modes, which are expected to sharpen and blueshift as the lattice hardens with

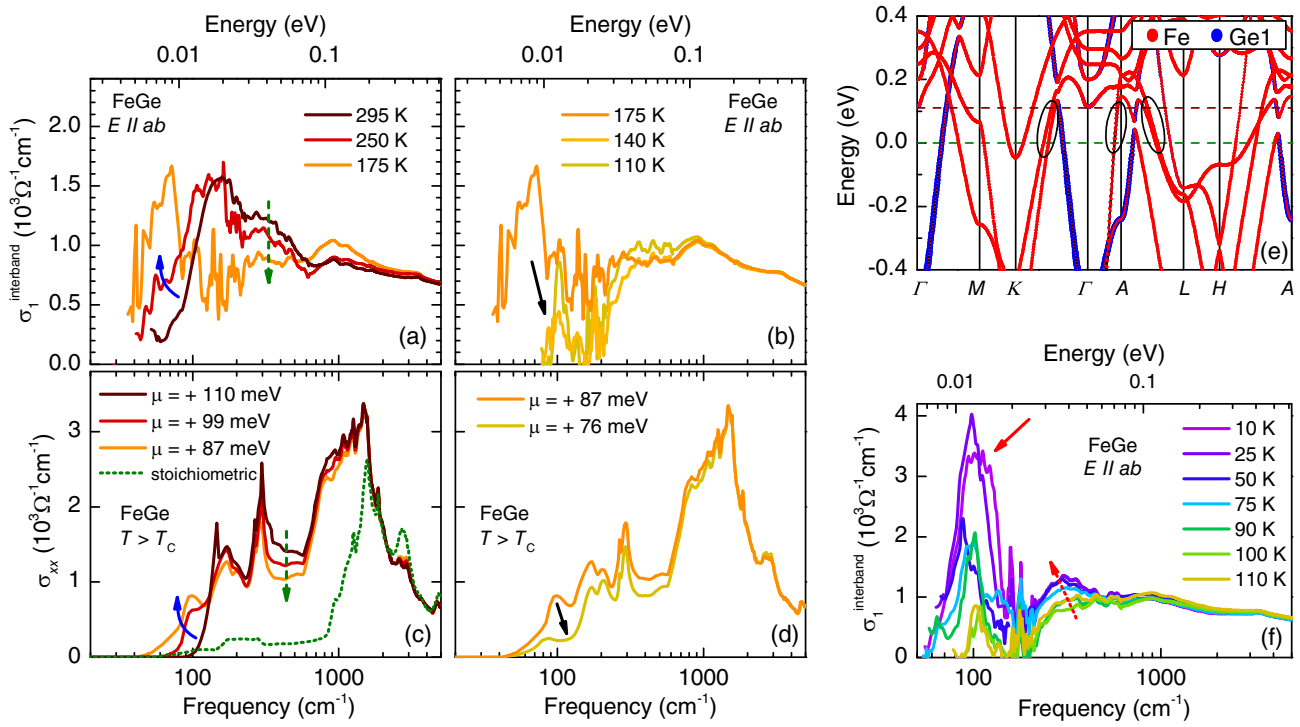

FIG. 2. (a),(b) Experimental interband transitions of FeGe at temperatures above T_C, obtained by subtracting the Drude and localization peaks and the Fano resonance from the optical conductivity. (c),(d) DFT in-plane optical conductivities for different electron dopings expressed by the chemical potential μ. The arrows mark characteristic changes in the spectra. (e) Calculated band structure for the high-temperature phase with colored dots symbolizing the contributions of different atoms. The black ovals highlight the linear Fe bands crossing the Fermi level responsible for the low-energy interband optical transitions. Dashed horizontal lines mark the position of the chemical potential for the stoichiometric case (green) and for $\mu = +110$ meV (brown), corresponding to room temperature. (f) Experimental interband transitions at temperatures below T_C. Red arrows mark the enhancement in the spectral weight at low energies due to the structural distortion.

decreasing temperature (see Supplemental Material for a more detailed discussion on the Fano resonance [34]). Second, there is a notable enhancement in the spectral weight around 250 cm^{-1} and a gradual formation of a sharp absorption feature at 100 cm^{-1}, as displayed in Fig. 2(f). However, no spectral weight transfer from low to high energies, i.e., no optical signature of a CDW gap, is observed. The absence of a gap opening in the optical spectra is consistent with the results of the Raman studies [56].

To further investigate the effect of lattice distortion below T_C on the electronic structure, we carry out DFT calculations of the band structure and optical conductivity for the low-temperature phase. Below T_C, a $2 \times 2 \times 2$ superstructure as depicted in Fig. 1(a), involving a trihexagonal (trh) distortion of the Fe-kagome planes was observed by x-ray diffraction (XRD) measurements [19]. Additionally, a partial dimerization of Ge1 atoms was proposed by XRD and inelastic x-ray scattering studies on annealed samples, as well as DFT simulations [24,25,57–59]. In both cases, however, the distortion of the kagome planes is on the order of 10^{-4} Å and, thus, extremely small.

The minuscule Fe displacement associated with the trihexagonal distortion induces only a tiny splitting between the parallel bands crossing the Fermi level (see Fig. S7 [34] for a more detailed view). Thus, plenty of spectral weight is found at low energies, resulting in the pronounced peak at 100 cm^{-1} as displayed in Fig. 3(b). The splitting between some parallel bands can be increased by imposing a larger displacement of the Fe atoms. As discussed in Supplemental Material [34], this leads to more spectral weight at energies between 200 and 1000 cm^{-1}, with the low-energy peak at 100 cm^{-1} persisting. However, there is still no indication of a gap opening either in the calculated optical conductivity or in the density of states, as shown in Fig. S6 [34]. Hence, our study suggests a different nature of the low-temperature transition in FeGe. Moreover, experimental manifestations of this transition appear to be dependent on the growth method and require sensitive measurements, as it was not detected in early studies [22,60]. Doping studies show a rapid suppression of the low-temperature anomaly in the magnetic susceptibility already at 1.5% Sb doping of the Ge sites, militating in favor of the significant involvement of the Ge atoms in the low-temperature phase transition [61].

The Ge dimerization has a more drastic effect on the band structure compared to the deformation of the kagome

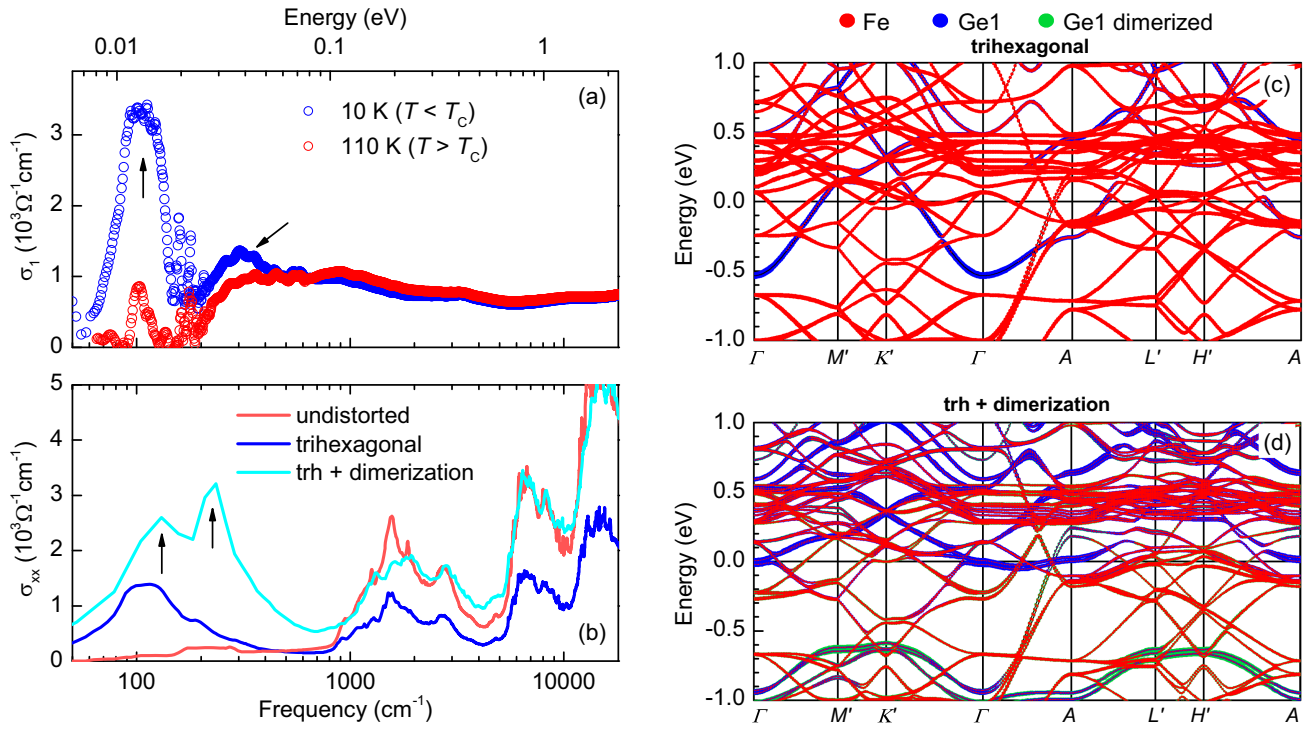

FIG. 3. (a) Experimental interband transitions of FeGe at 110 K (normal state) and 10 K (low-temperature state). (b) Calculated optical conductivity given for the normal state, as well as for the simple trihexagonal distortion of the kagome planes and the Ge-dimerized superstructure. The arrows mark the two low-energy absorption bands observed below T_C in the experimental data, which are reproduced by the calculations only when taking into account both the trihexagonal distortion of the Fe kagome layers and the partial dimerization of the Ge1 atoms. Band structures of the low-temperature state for (c) the trihexagonal distortion of the kagome planes and (d) the Ge-dimerized superstructure. Colored dots show the contributions of different atoms.

planes. As seen in Figs. 2(e) and 3(c), precisely one in-plane Ge1 band crosses the Fermi level in the normal state. This band becomes split in the dimerized state with a gap of around 0.7 eV [Fig. 3(d)]. While contributions from this splitting to the optical data are masked by several other interband optical transitions due to the multiband nature of FeGe, a reorganization of the Fe bands near E_F leads to additional spectral weight at approximately 250 cm^{-1}, consistent with the experimental result (Figs. 3(a) and 3(b)). Along with the improved agreement between theory and experiment above 1000 cm^{-1}, these findings support the Ge dimerization scenario. Furthermore, the involvement of Ge1 atoms may also explain why the low-temperature transition has rather strong signatures in the optical spectra, i.e., Fano anomalies and different interband transitions, even though almost no changes happen in the Fe-kagome planes.

The low-temperature anomaly in the magnetic susceptibility and the specific heat at T_C can be enhanced by a postgrowth annealing process. However, the signature of the corresponding phase transition in the electric resistivity remains astonishingly weak [24,25,56]. While additional Bragg peaks below T_C imply a structural modulation [19], this does not necessarily lead to a CDW. Kagome systems are prone to multiple structural instabilities, such as Wigner crystallization [9,14]. Moreover, breathing distortion of the kagome lattice is a well-known effect in quantum magnetism but also in the kagome metals where Fe_3Sn_2 adopts the breathing structure without any CDW [62–65].

Overall, there is a sharp contrast between FeGe and other kagome metals exhibiting a CDW at low temperatures, including the renowned AV_3Sb_5 compounds. Their kagome planes exhibit a very similar structural distortion at low temperatures, forming a 2×2 in-plane superstructure. However, being on the order of 10^{-1} Å, the deformation of the kagome layers is much more pronounced in the AV_3Sb_5 compounds [66]. Interestingly, in their normal state, all these kagome metals feature multiple d bands and exactly one p-band crossing the Fermi level. This p band is related to the in-plane Ge1 atoms in FeGe but to out-of-plane Sb2 atoms in AV_3Sb_5 [67]. It essentially remains intact in the CDW phase of AV_3Sb_5 [66] but splits in FeGe due to the partial dimerization of the in-plane Ge1 atoms. Lastly, our data do not reveal the presence of a gap in the low-temperature phase of FeGe, while clear signatures of a gap opening in ScV_6Sn_6 and the AV_3Sb_5 compounds were detected by infrared spectroscopy [51–53,68–71].

All these findings imply that the low-temperature phase of FeGe is substantially different from the CDW phase

observed in other kagome metals. On the one hand, our study supports the partial dimerization of the in-plane Ge atoms, being decisive for the significant changes in the optical data below T_C. On the other hand, the absence of a gap in both experiment and theory is clearly different from the conventional CDW scenario that has been discussed for FeGe previously. Given the complex interplay between magnetism, structural instabilities, and strong electronic correlations, as well as the simple tunability of the low-temperature anomaly by doping and annealing [24,25,56,61], antiferromagnetic FeGe might open new routes to study so far unexplored regions in the rich phase diagram of kagome metals.

The authors acknowledge the fruitful discussions with S. Fratini and the technical support by G. Untereiner. M. W. is supported by Center for Integrated Quantum Science and Technology (IQST) Stuttgart/Ulm via a project funded by the Carl Zeiss Stiftung. The work has been supported by the Deutsche Forschungsgemeinschaft (DFG) via DR228/51-3, DR228/68-1, and UY63/2-1.

*maxim.wenzel@pi1.physik.uni-stuttgart.de

[1] I. Syôzi, Statistics of kagomé lattice, Prog. Theor. Phys. **6**, 306 (1951).
[2] M. Mekata, Kagome: The story of the basketweave lattice, Phys. Today **56**, No. 2, 12 (2003).
[3] D. Kim and F. Liu, Realization of flat bands by lattice intercalation in kagome metals, Phys. Rev. B **107**, 205130 (2023).
[4] Z. Li, J. Zhuang, L. Wang, H. Feng, Q. Gao, X. Xu, W. Hao, X. Wang, C. Zhang, K. Wu, S. X. Dou, L. Chen, Z. Hu, and Y. Du, Realization of flat band with possible nontrivial topology in electronic Kagome lattice, Sci. Adv. **4**, eaau4511 (2018).
[5] M. L. Kiesel, C. Platt, and R. Thomale, Unconventional Fermi surface instabilities in the kagome Hubbard model, Phys. Rev. Lett. **110**, 126405 (2013).
[6] K. Ferhat and A. Ralko, Phase diagram of the $\frac{1}{3}$-filled extended Hubbard model on the kagome lattice, Phys. Rev. B **89**, 155141 (2014).
[7] T. Neupert, M. M. Denner, J.-X. Yin, R. Thomale, and M. Z. Hasan, Charge order and superconductivity in kagome materials, Nat. Phys. **18**, 137 (2022).
[8] F. Pollmann, P. Fulde, and K. Shtengel, Kinetic ferromagnetism on a kagome lattice, Phys. Rev. Lett. **100**, 136404 (2008).
[9] C. Wu, D. Bergman, L. Balents, and S. Das Sarma, Flat bands and Wigner crystallization in the honeycomb optical lattice, Phys. Rev. Lett. **99**, 070401 (2007).
[10] M. L. Kiesel and R. Thomale, Sublattice interference in the kagome Hubbard model, Phys. Rev. B **86**, 121105(R) (2012).
[11] S.-L. Yu and J.-X. Li, Chiral superconducting phase and chiral spin-density-wave phase in a Hubbard model on the kagome lattice, Phys. Rev. B **85**, 144402 (2012).
[12] Y.-P. Lin and R. M. Nandkishore, Complex charge density waves at Van Hove singularity on hexagonal lattices: Haldane-model phase diagram and potential realization in the kagome metals AV_3Sb_5 (A = K, Rb, Cs), Phys. Rev. B **104**, 045122 (2021).
[13] L. Nie, K. Sun, W. Ma, D. Song, L. Zheng, Z. Liang, P. Wu, F. Yu, J. Li, M. Shan, D. Zhao, S. Li, B. Kang, Z. Wu, Y. Zhou, K. Liu, Z. Xiang, J. Ying, Z. Wang, T. Wu, and X. Chen, Charge-density-wave-driven electronic nematicity in a kagome superconductor, Nature (London) **604**, 59 (2022).
[14] Y. Chen, S. Xu, Y. Xie, C. Zhong, C. Wu, and S. B. Zhang, Ferromagnetism and Wigner crystallization in kagome graphene and related structures, Phys. Rev. B **98**, 035135 (2018).
[15] B. R. Ortiz, L. C. Gomes, J. R. Morey, M. Winiarski, M. Bordelon, J. S. Mangum, I. W. H. Oswald, J. A. Rodriguez-Rivera, J. R. Neilson, S. D. Wilson, E. Ertekin, T. M. McQueen, and E. S. Toberer, New kagome prototype materials: Discovery of KV_3Sb_5, RbV_3Sb_5, and CsV_3Sb_5, Phys. Rev. Mater. **3**, 094407 (2019).
[16] H. Tan, Y. Liu, Z. Wang, and B. Yan, Charge density waves and electronic properties of superconducting kagome metals, Phys. Rev. Lett. **127**, 046401 (2021).
[17] M. M. Denner, R. Thomale, and T. Neupert, Analysis of charge order in the kagome metal AV_3Sb_5 (A = K, Rb, Cs), Phys. Rev. Lett. **127**, 217601 (2021).
[18] M. Kang, S. Fang, J. Yoo, B. R. Ortiz, Y. M. Oey, J. Choi, S. H. Ryu, J. Kim, C. Jozwiak, A. Bostwick, E. Rotenberg, E. Kaxiras, J. G. Checkelsky, S. D. Wilson, J.-H. Park, and R. Comin, Charge order landscape and competition with superconductivity in kagome metals, Nat. Mater. **22**, 186 (2022).
[19] X. Teng, L. Chen, F. Ye, E. Rosenberg, Z. Liu, J.-X. Yin, Y.-X. Jiang, J. S. Oh, M. Z. Hasan, K. J. Neubauer, B. Gao, Y. Xie, M. Hashimoto, D. Lu, C. Jozwiak, A. Bostwick, E. Rotenberg, R. J. Birgeneau, J.-H. Chu, M. Yi, and P. Dai, Discovery of charge density wave in a kagome lattice antiferromagnet, Nature (London) **609**, 490 (2022).
[20] X. Teng, J. S. Oh, H. Tan, L. Chen, J. Huang, B. Gao, J.-X. Yin, J.-H. Chu, M. Hashimoto, C. Lu, Donghui Jozwiak, A. Bostwick, E. Rotenberg, G. E. Granroth, B. Yan, R. J. Birgeneau, P. Dai, and M. Yi, Magnetism and charge density wave order in kagome FeGe, Nat. Phys. **19**, 814 (2023).
[21] J.-X. Yin, Y.-X. Jiang, X. Teng, M. S. Hossain, S. Mardanya, T.-R. Chang, Z. Ye, G. Xu, M. M. Denner, T. Neupert, B. Lienhard, H.-B. Deng, C. Setty, Q. Si, G. Chang, Z. Guguchia, B. Gao, N. Shumiya, Q. Zhang, T. A. Cochran, D. Multer, M. Yi, P. Dai, and M. Z. Hasan, Discovery of charge order and corresponding edge state in kagome magnet FeGe, Phys. Rev. Lett. **129**, 166401 (2022).
[22] J. Bernhard, B. Lebech, and O. Beckman, Neutron diffraction studies of the low-temperature magnetic structure of hexagonal FeGe, J. Phys. F **14**, 2379 (1984).
[23] J. Bernhard, B. Lebech, and O. Beckman, Magnetic phase diagram of hexagonal FeGe determined by neutron diffraction, J. Phys. F **18**, 539 (1988).
[24] Z. Chen, X. Wu, S. Zhou, J. Zhang, R. Yin, Y. Li, M. Li, J. Gong, M. He, Y. Chai, X. Zhou, Y. Wang, A. Wang, Y.-J. Yan, and D.-L. Feng, Long-ranged charge order conspired

by magnetism and lattice in an antiferromagnetic kagome metal, arXiv:2307.07990.

[25] C. Shi, Y. Liu, B. B. Maity, Q. Wang, S. R. Kotla, S. Ramakrishnan, C. Eisele, H. Agarwal, L. Noohinejad, Q. Tao, B. Kang, Z. Lou, X. Yang, Y. Qi, X. Lin, Z.-A. Xu, A. Thamizhavel, G.-H. Cao, S. van Smaalen, S. Cao, and J.-K. Bao, Disordered structure for long-range charge density wave order in annealed crystals of magnetic kagome FeGe, arXiv:2308.09034.

[26] S. Wu, M. Klemm, J. Shah, E. T. Ritz, C. Duan, X. Teng, B. Gao, F. Ye, M. Matsuda, F. Li, X. Xu, M. Yi, T. Birol, P. Dai, and G. Blumberg, Symmetry breaking and ascending in the magnetic kagome metal FeGe, Phys. Rev. X **14**, 011043 (2024).

[27] Y. Huang, H. P. Wang, W. D. Wang, Y. G. Shi, and N. L. Wang, Formation of the density wave energy gap in $Na_2Ti_2Sb_2O$: An optical spectroscopy study, Phys. Rev. B **87**, 100507(R) (2013).

[28] W. J. Ban, H. P. Wang, C. W. Tseng, C. N. Kuo, C. S. Lue, and N. L. Wang, Revealing multiple charge-density-wave orders in $TbTe_3$ by optical conductivity and ultrafast pump-probe experiments, Sci. China Phys. Mech. Astron. **60**, 047011 (2017).

[29] V. Vescoli, L. Degiorgi, H. Berger, and L. Forró, Dynamics of correlated two-dimensional materials: The $2H - TaSe_2$ case, Phys. Rev. Lett. **81**, 453 (1998).

[30] R. Y. Chen, S. J. Zhang, M. Y. Zhang, T. Dong, and N. L. Wang, Revealing extremely low energy amplitude modes in the charge-density-wave compound $LaAgSb_2$, Phys. Rev. Lett. **118**, 107402 (2017).

[31] R. Y. Chen, B. F. Hu, T. Dong, and N. L. Wang, Revealing multiple charge-density-wave orders in $TbTe_3$ by optical conductivity and ultrafast pump-probe experiments, Phys. Rev. B **89**, 075114 (2014).

[32] F. Pfuner, P. Lerch, J.-H. Chu, H.-H. Kuo, I. R. Fisher, and L. Degiorgi, Temperature dependence of the excitation spectrum in the charge-density-wave $ErTe_3$ and $HoTe_3$ systems, Phys. Rev. B **81**, 195110 (2010).

[33] A. Perucchi, L. Degiorgi, and R. E. Thorne, Optical investigation of the charge-density-wave phase transitions in $NbSe_3$, Phys. Rev. B **69**, 195114 (2004).

[34] See Supplemental Material at http://link.aps.org/supplemental/10.1103/PhysRevLett.132.266505 for experimental details, data analysis, details on DFT calculations, and additional computational results, which includes Refs. [35–46].

[35] M. W. Richardson, N. Ingri, P. Salomaa, G. D. Bloom, and G. Hagen, The partial equilibrium diagram of the Fe-Ge system in the range 40-72 at.% Ge, and the crystallisation of some iron germanides by chemical transport reactions, Acta Chem. Scand. **21**, 2305 (1967).

[36] C. C. Homes, M. Reedyk, D. A. Cradles, and T. Timusk, Technique for measuring the reflectance of irregular, submillimeter-sized samples, Appl. Opt. **32**, 2976 (1993).

[37] D. B. Tanner, Use of x-ray scattering functions in Kramers-Kronig analysis of reflectance, Phys. Rev. B **91**, 035123 (2015).

[38] P. Blaha, K. Schwarz, G. Madsen, D. Kvasnicka, J. Luitz, R. Laskowski, F. Tran, and L. Marks, *WIEN2k, An Augmented Plane Wave+Local Orbitals Program for Calculating Crystal Properties* (Karlheinz Schwarz, Techn. Universität Wien, Austria, 2018), ISBN 3-9501031-1-2.

[39] P. Blaha, K. Schwarz, F. Tran, R. Laskowski, G. K. H. Madsen, and L. D. Marks, WIEN2k: An APW + lo program for calculating the properties of solids, J. Chem. Phys. **152**, 074101 (2020).

[40] J. P. Perdew, K. Burke, and M. Ernzerhof, Generalized gradient approximation made simple, Phys. Rev. Lett. **77**, 3865 (1996).

[41] G. Kresse and J. Furthmüller, Efficient iterative schemes for *ab initio* total-energy calculations using a plane-wave basis set, Phys. Rev. B **54**, 11169 (1996).

[42] C. Ambrosch-Draxl and J. O. Sofo, Linear optical properties of solids within the full-potential linearized augmented planewave method, Comput. Phys. Commun. **175**, 1 (2006).

[43] S. Fratini, S. Ciuchi, and D. Mayou, Phenomenological model for charge dynamics and optical response of disordered systems: Application to organic semiconductors, Phys. Rev. B **89**, 235201 (2014).

[44] H. Rammal, A. Ralko, S. Ciuchi, and S. Fratini, Transient localization from the interaction with quantum bosons, Phys. Rev. Lett. **132**, 266502 (2024).

[45] M. Kawamura, FermiSurfer: Fermi-surface viewer providing multiple representation schemes, Comput. Phys. Commun. **239**, 197 (2019).

[46] Y. Shao, A. N. Rudenko, J. Hu, Z. Sun, Y. Zhu, S. Moon, A. Millis, S. Yuan, A. I. Lichtenstein, D. Smirnov, Z. Q. Mao, M. I. Katsnelson, and D. N. Basov, Electronic correlations in nodal-line semimetals, Nat. Phys. **16**, 636 (2020).

[47] A. Biswas, O. Iakutkina, Q. Wang, H. C. Lei, M. Dressel, and E. Uykur, Spin-reorientation-induced band gap in Fe_3Sn_2: Optical signatures of Weyl nodes, Phys. Rev. Lett. **125**, 076403 (2020).

[48] F. Schilberth, N. Unglert, L. Prodan, F. Meggle, J. Ebad Allah, C. A. Kuntscher, A. A. Tsirlin, V. Tsurkan, J. Deisenhofer, L. Chioncel, I. Kézsmárki, and S. Bordács, Magneto-optical detection of topological contributions to the anomalous Hall effect in a kagome ferromagnet, Phys. Rev. B **106**, 144404 (2022).

[49] M. Wenzel, A. A. Tsirlin, O. Iakutkina, Q. Yin, H. C. Lei, M. Dressel, and E. Uykur, Effect of magnetism and phonons on localized carriers in the ferrimagnetic kagome metals $GdMn_6Sn_6$ and $TbMn_6Sn_6$, Phys. Rev. B **106**, L241108 (2022).

[50] K. Momma and F. Izumi, VESTA: A three-dimensional visualization system for electronic and structural analysis, J. Appl. Crystallogr. **41**, 653 (2008).

[51] M. Wenzel, B. R. Ortiz, S. D. Wilson, M. Dressel, A. A. Tsirlin, and E. Uykur, Optical study of RbV_3Sb_5: Multiple density-wave gaps and phonon anomalies, Phys. Rev. B **105**, 245123 (2022).

[52] E. Uykur, B. R. Ortiz, S. D. Wilson, M. Dressel, and A. A. Tsirlin, Optical detection of the density-wave instability in the kagome metal KV_3Sb_5, npj Quantum Mater. **7**, 16 (2022).

[53] E. Uykur, B. R. Ortiz, O. Iakutkina, M. Wenzel, S. D. Wilson, M. Dressel, and A. A. Tsirlin, Low-energy optical properties of the nonmagnetic kagome metal CsV_3Sb_5, Phys. Rev. B **104**, 045130 (2021).

[54] M. Wenzel, A. A. Tsirlin, F. Capitani, Y. T. Chan, B. R. Ortiz, S. D. Wilson, M. Dressel, and E. Uykur, Pressure evolution of electron dynamics in the superconducting kagome metal CsV_3Sb_5, npj Quantum Mater. **8**, 45 (2023).

[55] Y. Xu, J. Zhao, C. Yi, Q. Wang, Q. Yin, Y. Wang, X. Hu, L. Wang, E. Liu, G. Xu, L. Lu, A. A. Soluyanov, H. Lei, Y. Shi, J. Luo, and Z.-G. Chen, Electronic correlations and flattened band in magnetic Weyl semimetal candidate $Co_3Sn_2S_2$, Nat. Commun. **11**, 3985 (2020).

[56] X. Wu, X. Mi, L. Zhang, X. Zhou, M. He, Y. Chai, and A. Wang, Annealing-tunable charge density wave order in a magnetic kagome material FeGe, Phys. Rev. Lett. **132**, 256501 (2024).

[57] Y. Wang, Enhanced spin-polarization via partial Ge-dimerization as the driving force of the charge density wave in FeGe, Phys. Rev. Mater. **7**, 104006 (2023).

[58] S. Shao, J.-X. Yin, I. Belopolski, J.-Y. You, T. Hou, H. Chen, Y. Jiang, M. S. Hossain, M. Yahyavi, C.-H. Hsu, Y. P. Feng, A. Bansil, M. Z. Hasan, and G. Chang, Intertwining of magnetism and charge ordering in kagome FeGe, ACS Nano **17**, 10164 (2023).

[59] H. Miao, T. T. Zhang, H. X. Li, G. Fabbris, A. H. Said, R. Tartaglia, T. Yilmaz, E. Vescovo, J.-X. Yin, S. Murakami, X. L. Feng, K. Jiang, X. L. Wu, A. F. Wang, S. Okamoto, Y. L. Wang, and H. N. Lee, Signature of spin-phonon coupling driven charge density wave in a kagome magnet, Nat. Commun. **14**, 6183 (2023).

[60] O. Beckman, K. Carrander, L. Lundgren, and M. Richardson, Susceptibility measurements and magnetic ordering of hexagonal FeGe, Phys. Scr. **6**, 151 (1972).

[61] J. Huang, C. Shang, J. Qin, F. Pan, B. Shi, J. Wang, J. Liu, D. Xu, H. Zhang, H. Wang, L. Hao, and P. Cheng, $FeGe_{1-x}Sb_x$: A series of novel kagome metals with noncollinear antiferromagnetism, Phys. Rev. B **108**, 184431 (2023).

[62] R. Schaffer, Y. Huh, K. Hwang, and Y. B. Kim, Quantum spin liquid in a breathing kagome lattice, Phys. Rev. B **95**, 054410 (2017).

[63] H. Tanaka, Y. Fujisawa, K. Kuroda, R. Noguchi, S. Sakuragi, C. Bareille, B. Smith, C. Cacho, S. W. Jung, T. Muro, Y. Okada, and T. Kondo, Three-dimensional electronic structure in ferromagnetic Fe_3Sn_2 with breathing kagome bilayers, Phys. Rev. B **101**, 161114(R) (2020).

[64] M. Hirschberger, T. Nakajima, S. Gao, L. Peng, A. Kikkawa, T. Kurumaji, M. Kriener, Y. Yamasaki, H. Sagayama, H. Nakao, K. Ohishi, K. Kakurai, Y. Taguchi, X. Yu, T.-h. Arima, and Y. Tokura, Three-dimensional electronic structure in ferromagnetic Fe_3Sn_2 with breathing kagome bilayers, Nat. Commun. **10**, 5831 (2019).

[65] S. Regmi, T. Fernando, Y. Zhao, A. P. Sakhya, G. Dhakal, I. Bin Elius, H. Vazquez, J. D. Denlinger, J. Yang, J.-H. Chu, X. Xu, T. Cao, and M. Neupane, Spectroscopic evidence of flat bands in breathing kagome semiconductor Nb_3I_8, Commun. Mater. **3**, 100 (2022).

[66] B. R. Ortiz, S. M. L. Teicher, L. Kautzsch, P. M. Sarte, N. Ratcliff, J. Harter, J. P. C. Ruff, R. Seshadri, and S. D. Wilson, Fermi surface mapping and the nature of charge-density-wave order in the kagome superconductor CsV_3Sb_5, Phys. Rev. X **11**, 041030 (2021).

[67] A. A. Tsirlin, P. Fertey, B. R. Ortiz, B. Klis, V. Merkl, M. Dressel, S. D. Wilson, and E. Uykur, Role of Sb in the superconducting kagome metal CsV_3Sb_5 revealed by its anisotropic compression, SciPost Phys. **12**, 49 (2022).

[68] T. Hu, H. Pi, S. Xu, L. Yue, Q. Wu, Q. Liu, S. Zhang, R. Li, X. Zhou, J. Yuan, D. Wu, T. Dong, H. Weng, and N. Wang, Optical spectroscopy and band structure calculations of the structural phase transition in the vanadium-based kagome metal ScV_6Sn_6, Phys. Rev. B **107**, 165119 (2023).

[69] D. W. Kim, S. Liu, C. Wang, H. W. Nam, G. Pokharel, S. D. Wilson, J.-H. Cho, and S. J. Moon, Infrared probe of the charge density wave gap in ScV_6Sn_6, Phys. Rev. B **108**, 205118 (2023).

[70] X. Zhou, Y. Li, X. Fan, J. Hao, Y. Dai, Z. Wang, Y. Yao, and H.-H. Wen, Origin of charge density wave in the kagome metal CsV_3Sb_5 as revealed by optical spectroscopy, Phys. Rev. B **104**, L041101 (2021).

[71] X. Zhou, Y. Li, X. Fan, J. Hao, Y. Xiang, Z. Liu, Y. Dai, Z. Wang, Y. Yao, and H.-H. Wen, Electronic correlations and evolution of the charge density wave in the kagome metals AV_3Sb_5 $(A = \mathrm{K}, \mathrm{Rb}, \mathrm{Cs})$, Phys. Rev. B **107**, 165123 (2023).